City Research Online

City, University of London Institutional Repository

This is the accepted version of the paper.

This version of the publication may differ from the final published version.

Effect of End-Wall Riblets on radial Turbine Performance

M A Khader
City, University of London, UK
Mahmoud.khader.1@city.ac.uk
A I Sayma
City, University of London, UK
a.sayma@city.ac.uk

Abstract

This paper presents a detailed study of the impact of manufacturing residual riblets at the rotor hub surface of a radial inflow turbine on the flow within the rotor passages and their contribution to drag reduction. Numerical analysis has been used to study the effects of those features at design point conditions. Riblets with different height and spacing have been examined to determine the riblet geometry where the maximum drag reduction is achieved. The relative height of the riblets to rotor inlet blade height was introduced to generalise the results. At the end of this study the results were compared with the available data in literature. It was found that the introduction of riblets could reduce the wall shear stress at the hub surface, while they contribute to increasing the streamwise vorticity within the rotor passage. For the geometries tested, the minimum drag was achieved using riblets with relative height $h_{rel} = 2.5\%$ equivalent to 19.3 wall units. The results revealed that the spacing between riblets have a minor effect on their performance, this is due to the size of the streamwise vortex above the hub surface which will be discussed in this work.

1.1 Introduction

Flow within the radial turbine rotors is highly three-dimensional and is combined with strong secondary flows, which become more complicated near the passages walls. The interaction between the turbulent boundary layer and the solid surfaces affects the boundary layer development and causes energy losses due to skin friction drag. Surface roughness is one of the important factors that affect the flow within the boundary layer. Therefore it is necessary to study the effects of the manufacturing residual riblets on the losses within the turbine rotor. The improved understanding could lead to the introduction of intentional riblets that are increasingly becoming feasible with the fast development of three dimensional printing technology of components. Different studies have proved that smooth surfaces do not necessarily have less drag than rough surfaces [1, 2, 3, 4]. Riblets are surface structures arranged in the streamwise direction to help in reducing wall shear stresses. They can have different shapes and arrangements as shown in figure 1. Walsh [3] studied the effect of

different riblet shapes on drag reduction over flat plate surface, where 8% drag reduction was achieved using V-shaped riblets. By adding V-shaped riblets to the blades of axial compressor cascade, Oehlert et al. [5] achieved 3.6% reduction in total pressure loss. Feng et al. [6] conducted an experiment to test the effectiveness of riblets in drag reduction where they achieved 10% drag reduction by adding the riblets to the pressure surface of an axial compressor cascade.
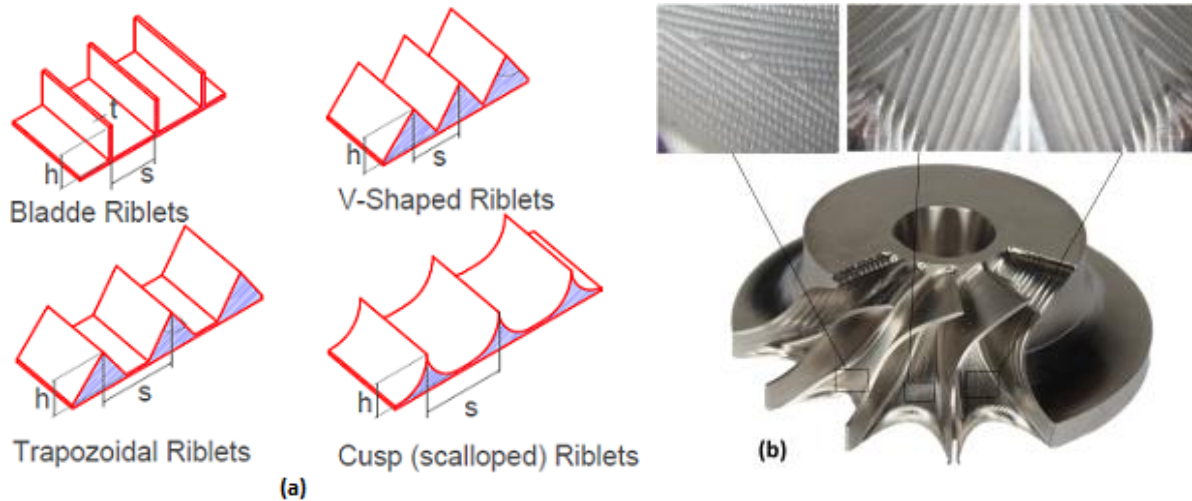

Figure (1): (a) Different riblet configurations (b) Turbine rotor with three different hub surface finish

They also noticed that this reduction in drag is insensitive to the flow incidence angle. On the contrast, Bushan et al. [7] found that adding riblets to a straight rectangular duct has a negative impact on drag. In their experiment, blade shape riblets with different heights and spacing were attached to the duct wall, and the pressure drop was measured across the duct for range of flow velocities. For all riblets arrangements and along the speed range the pressure drop was higher compared to the surface without riblets. Zhang et al. [8] explored the effects of adding riblets to an axial turbine hub cascade experimentally. The grooves of the Riblets were machined in the streamwise direction. The study revealed that riblets can reduce pressure side of the horse-shoe vortex, and alleviate the growth of the passage vortex. Kim et al. [9] introduced a single rectangular fence in a 90° turning to mimic the effect of riblets on turbine passage. The mass-weighted average total pressure loss in the duct with fence was reduced by 8.6% relative to the duct without the fence. Miao et al. [10] found that introducing riblets with different shapes and density to a 90° duct alleviates the stream wise vorticity compared to smooth walls duct. Riblets concept has been also applied to radial turbomachines. Where Lei et al. [1] tested a centrifugal compressor with different machining residual riblets heights on the impeller hub. They found that using riblets decreases wall shear

stress which reaches its minimum value for riblets of height 0.58 relative to impeller exit blade width.

Walsh [3] investigated the effectiveness of several riblet geometries on drag reduction where he found that the highest drag reduction could be achieved using riblets with cusp shape. In a different study, Oehlert et al. [5] found that riblets with blade shape has greater effect on drag reduction over the cusp shaped riblets. Nonetheless, blade riblets can neither be machined nor they would withstand high stresses. Moreover, the residual surfaces resulted from the actual machining process of the turbine rotor are very similar to cusp riblets. Figure 1b shows rotor sample machined using ball end cutter milling with different surface finish, where cusp riblets are clear in the magnified surfaces. So, for practical reasons, the present work focused on studying the effect of cusp shape riblets.

To the knowledge of the authors, the effects of the residual surface structures on the radial turbines performance were not addressed before, therefore it was important to include riblets with different geometry in the study. It is understood from the literature that the main geometrical parameters that affect the riblets performance are the height of the riblets and the spacing between them. Therefore, riblets with different heights (h) and spacing (s) were introduced to the hub surface of a turbine rotor designed for 6 kWe micro gas turbine. The turbine stage was then analysed numerically at design point. Table 1 lists the turbine operational conditions and figure 2 shows the main geometrical parameters for the rotor.

Table 1: Turbine specifications

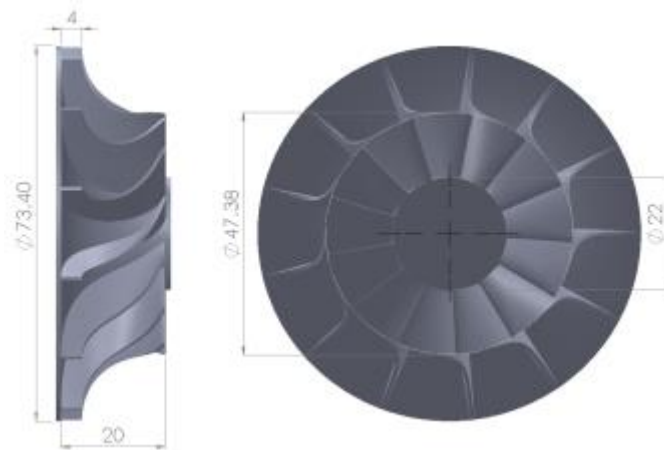| Parameter	Value
Total Pressure Ratio (bar)	3
Turbine inlet total temperature (K)	1073
Turbine mass flow rate (kg/s)	0.09
Power generated by turbine (kW)	21
Rotational speed (rpm)	130,000

Figure (2): rotor dimensions [mm]

To generalise the results of the study, the dimensionless parameter h_{rel} was introduced to characterise the size of the riblets. h_{rel} is defined as the percentage ratio of the cusp height h to the rotor inlet blade height b (figure 3). The space between riblets was defined using the polar angle ($\emptyset$) between the adjacent riblets as the area of the passage is changing along the streamwise direction. Thus, the distance s can be calculated at certain radius of the hub as:

$$s = r_{hub}\emptyset \tag{1}$$

The detailed dimensions for the riblets used in this study are summarised in Table 2.

The computational domain included a single rotor passage and single Nozzle Guide Vanes (NGVs) passage. The commercial tool ANSYS TurboGrid was used to generate hexahedral structured mesh for the stator vane, where ANSYS Workbench was used to generate unstructured mesh for the rotor.
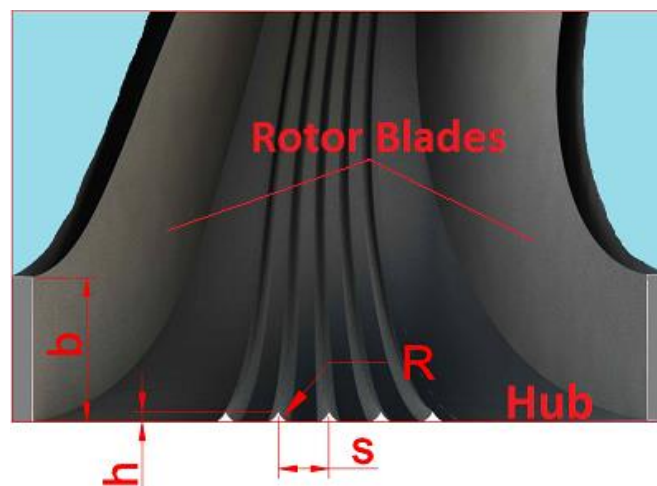

Figure (3): Riblets terminology

CFD computations were performed using ANSYS CFX 15.0. CFX is Reynolds Averaged Navier Stokes (RANS) based solver which solve the flow equations using finite volume

formulation. The flow was assumed to be fully turbulent due to high Reynolds number in the rotor passage. The Reynolds number was calculated assuming a rectangular duct, therefore using the passage hydraulic diameter, the Reynolds number at the design point was 27000. Dai et al. [11], found that turbulence intensity along the rotor passage does not exceed 7%, so 5% has been used in this work. The Shear Stress Transport (SST) turbulence model was used as it showed a good agreement with the experimental data for radial turbines in previous studies [12, 13].

Non-slip boundary condition was set for the passage surfaces. To solve the boundary layer accurately, the near wall mesh was refined to achieve first node non-dimensional distance $y^+ = 1$. Stage connection (mixing plane) was used between the rotor and stator, where all fluxes are averaged through the interfaces surfaces. Uniform total pressure and temperature were set at the domain inlet and uniform static pressure at the domain outlet. As one vane and one rotor blade passage were used, rotational periodicity was imposed on the periodic boundaries. Using this setup, CFX was run for a steady state solution.

Table 1: riblets dimensions

h [mm]	h_{rel} [mm]	R [mm]	s [3 riblets] $\emptyset = 4.45°$	s [5 riblets] $\emptyset = 2.2°$	s [10 riblets] $\emptyset = 1.1°$
0.06	1.5%	0.8	$0.078r_{hub}$	$0.039r_{hub}$	$0.019r_{hub}$
0.1	2.5%	0.6	$0.078r_{hub}$	$0.039r_{hub}$	$0.019r_{hub}$
0.2	5%	0.6	$0.078r_{hub}$	$0.039r_{hub}$	$0.019r_{hub}$

Grid independence check was performed for both numerical domains (smooth and ribbed rotors). For the rotor with riblets, the grid independence study was performed on the rotor with the highest cusp and smallest space as it requires the highest quantity of grid nodes to model those features. Using five grids of increasing refinement, the absolute vorticity, mass flow rate, flow velocities and angels at rotor inlet and outlet were calculated and compared. The For the domain with riblets, the girds density varied between 400,000 and 2 million nodes, and for the rotor without riblets, the this was between 0.4-1.7 million nodes. Figure 4 shows the error percentage in calculating the vorticity referring to the value generated using the finest grid. Vorticity showed the highest sensitivity to grid refinement, this is due to the small turbulent structures that needed fine mesh to be captured. For the domain with riblets the error is reduced to less than 1% with the mesh of 1.2 million nodes, and for the domain without riblets the error is reduced to less than 0.9% using the grid with 900k nodes. The final mesh for both rotors is shown in figure 5.
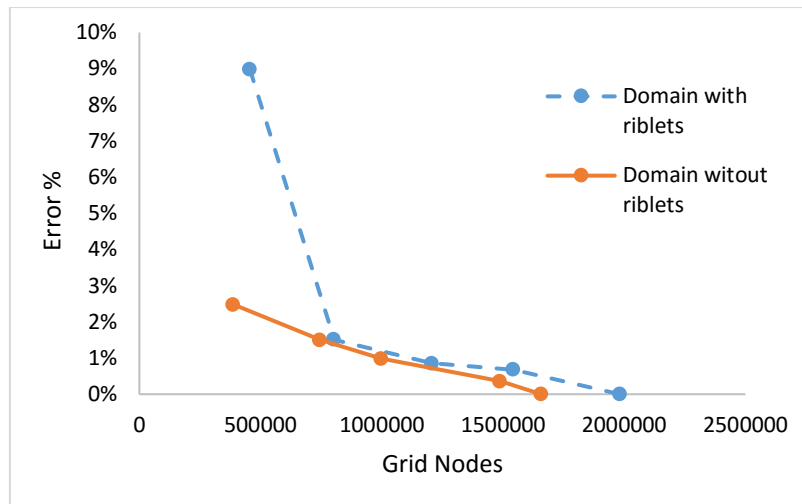
Figure (4): Grid independence study for computational domain with riblets

1.2 Validation of the CFD methodology

To verify the accuracy of the numerical method used, flow solutions were compared with experimental data. Experimental studies describing the flow within the turbine rotor are scarce. One of the main reasons for that, is difficulty to insert measuring instruments and the lack of the optical access to the rotor passage. Also, the high operating temperatures is another obstacle in front of using different flow visualisation techniques. Moreover, most of the published experiments does not have an adequate information to regenerate the geometry. Jones [14] provided the experimental data and the geometry description for the turbine used in Sundstrand Power Systems T-100 Multipurpose Power Unit. The turbine generates 50 hp at pressure ratio 5.5 and a turbine inlet temperature 1056 k while running at 105,600 rpm which is very close to the turbine used in this study.
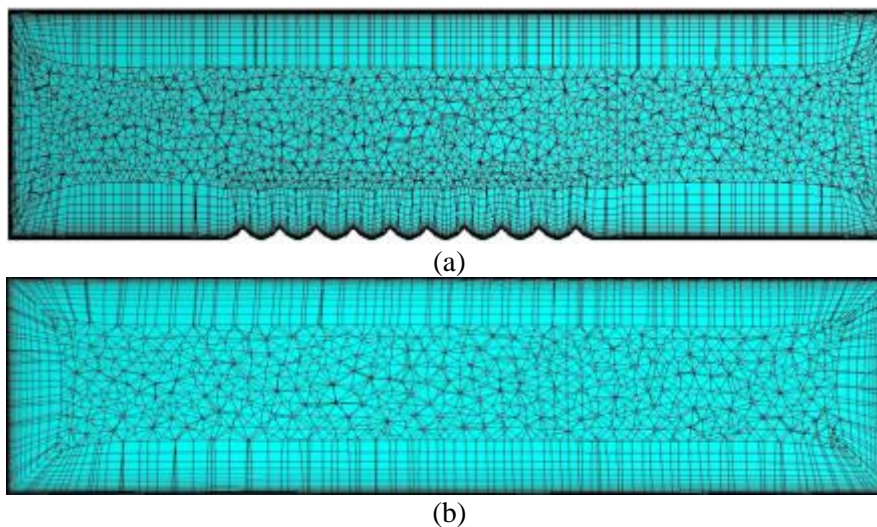

(a)

(b)

Figure (5): Computational grid (a) rotor passage with riblets (b) rotor passage without riblets

The absolute flow angles at the rotor exit are compared in figure 6a, where CFD results show a good agreement with the experimental results. However, CFD predictions deviate from the experimental near the tip region. This difference could be due to the rotor back-face clearance flow which was not included in the numerical domain. Sun et al. [15] noticed similar deviation in the flow angle predicted using CFD when they studied the effects of back-face clearance gap on the flow in the turbine passage. Figure 6b shows a comparison between CFD and test rig results for the span-wise distribution of meridional velocity at the rotor exit. It can be noticed that the difference between the values is almost constant, which means that this deviation is related to the over estimation of the mass flow in the CFD analysis.

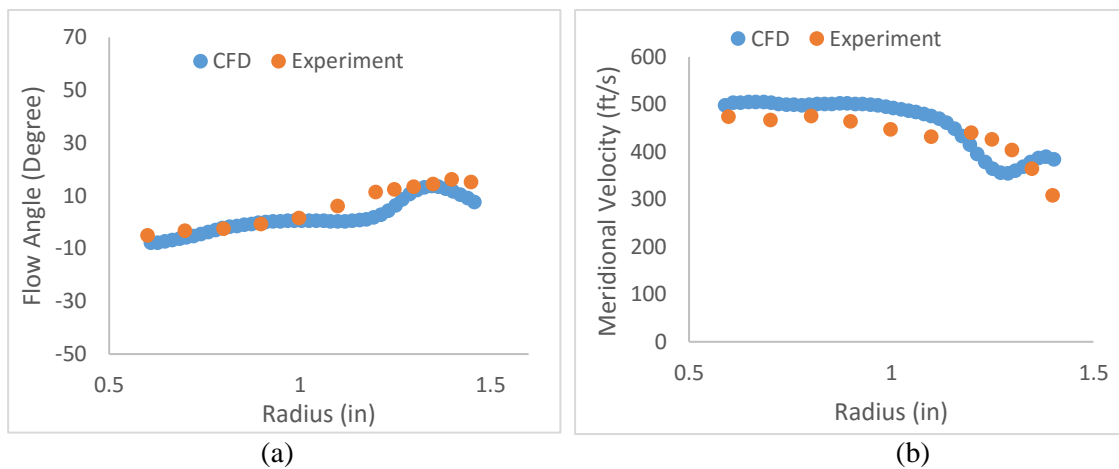(a)   (b)

Figure (6): Spanwise distribution of (a) flow angle (b) meridional velocity at rotor discharge

This could be because of the assumption of smooth profile of the turbine components, which will reduce the boundary layer blockage allowing more flow to pass. Moreover, during the test, the flow is expected to leak through the back-face seal of the turbine which could reach up to 1% of mass flow. Generally, the simulation results agree with the experimental data. Therefore, the present CFD methodology was considered to be suitable to study the flow behaviour through the turbine rotor, and is capable to demonstrate the effect of adding riblets on the turbine performance.

1.3 Results and Discussion

This section presents a description for the secondary flow motion in radial turbine passage, operating mechanism of riblets and comparison of different riblets geometries on drag reduction.

1.3.1 Secondary Flow in the Radial Turbine Rotor

In the literature; authors divided secondary flow characteristics in a turbine rotor into three categories based on their location along the passage. At the inlet section where the flow is purely radial, Coriolis acceleration has a very large effect on the low momentum fluid at the hub and shroud; therefore it acts to move flow from the Pressure Surface (PS) to the Suction Surface (SS) where the reduced static pressure $(P_r = P_s - \frac{1}{2}\rho\omega^2 r^2)$ is minimum. Along the rotor bend, where the flow starts to change its direction from radial to axial, secondary flows are generated because of both passage rotation and curvature. Coriolis acceleration is responsible for the movement of the low energy fluid from PS to the SS at the hub and shroud surfaces. Also, the passage curvature acts to move the low energy fluid at the pressure and suction surfaces from hub to shroud. For a fluid particle that is moving along the bend with a particular velocity there is a pressure gradient acting normal to its direction of motion to balance the centrifugal force on it. This pressure gradient is constant along the spanwise direction while the near wall fluid particles have a lower velocity than particles in the free stream. This difference in velocity causes the near wall particles to move toward the inner curve to reduce the radius of curvature [16]. Towards the end of this section, the secondary vortices at the hub start to move towards the top middle of the passage.

At the exducer section, the rotor passage is curved in the tangential direction. This curvature causes the low momentum fluid at the hub and shroud to swipe towards the SS where the curvature radius is minimum. Also, the radial component of the Coriolis acceleration causes a movement of the low energy fluids at the PS and SS from hub to shroud. In this section the secondary vortices accumulate in middle and top parts of the passage close to the suction surface. Figure 7 illustrates the motion of the low momentum flows at the different sections of the rotor passage [17].
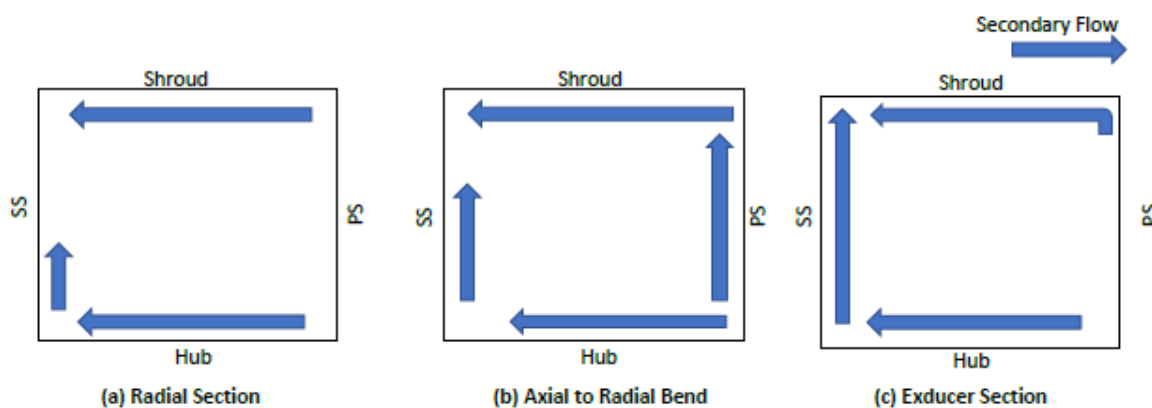
Figure (7): Secondary flow motion along turbine rotor passage

1.3.2 Riblets Operating Mechanism

To understand the operating mechanism of riblets, the flow structure is compared between ribbed and smooth hub rotor passage. In this section the smooth hub surface was compared with surface with 5 riblets of h_{rel} 2.5%. Figure 10 shows the cross-flow motion at the hub surface at 40% cross plane. It can be noticed that the cross-stream flow interacts with the riblets at the hub surface impeding it movement and generating secondary vortices that prevent the streamwise vortex from moving inside riblets valley. This will retain the slow fluids inside riblets valley thus the momentum exchange in the boundary layer is reduced. The interaction between the stream wise vortex and the low momentum fluid close to the hub causes high local shear at the rotor hub surface. By introducing riblets to the wall, this vortex is shifted from the wall to interact with the riblets tips.
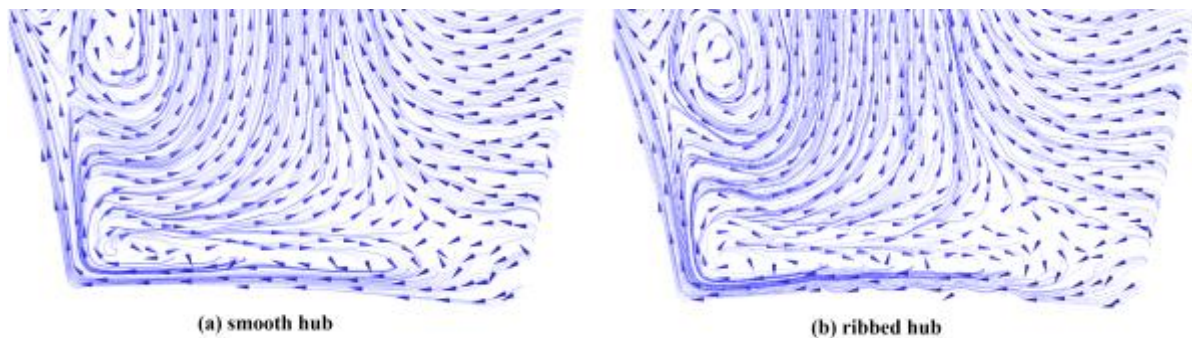

(a) smooth hub   (b) ribbed hub

Figure (10): effect of riblets on cross stream motion of the low energy fluids near the hub surface

This interaction generates secondary vortices which weaken the streamwise vortex by interfering with the cross-stream motion of the low momentum fluids at the hub surface and keeps the streamwise vortex away from the wall. This reduction of the cross-flow fluctuation and shifting the streamwise vortex away from the wall reduces the turbulent momentum transfer which results in reducing skin friction. The limiting streamlines (velocity streamlines at a distance normal to the wall approaching zero) at the hub surface in figure 11a shows the strong relative motion of the low energy fluids at the hub surface. Introducing riblets to the hub surface (figure 11b) form an obstacle which retards the cross-stream motion and tries to align them in the streamwise direction.
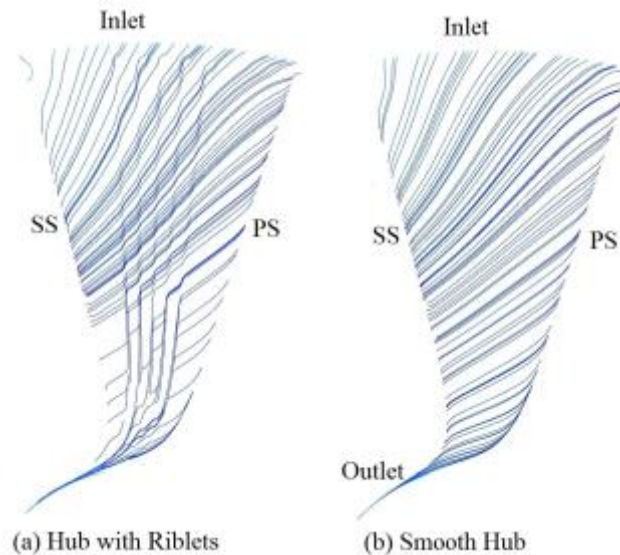
Figure (11): Limiting streamlines at the rotor hub

In figure 12, the Q-criterion method was used to visualise the streamwise vortex over smooth and ribbed hub surfaces at 40% cross plane. As it can be seen; the interaction between the cross flows and the riblet tips generates secondary vortices that weaken the streamwise vortex and form a barrier that lifts it from the hub surface.

Figure (12): Stream-wise vortex structure over hub surface

The mass averaged vorticity normalised by multiplying by (Inlet blade height (b)/ Inlet flow velocity) is presented in figure 13. The vorticity value shows a noticeable reduction inside the riblets valley compared to the smooth surface which confirms that riblets weaken the streamwise vortex close to hub surface. However, the vorticity at the outer region of the riblets valley is slightly higher because of the secondary vortices generated at the riblets tip. At the tip region, the vorticity reaches its maximum value in the region where the secondary vortices are located. Nonetheless the secondary vortex close to riblet tip does not have a significant effect on increasing skin friction as the vortex size is relatively small and it interacts with very small area at the peak of the riblet.
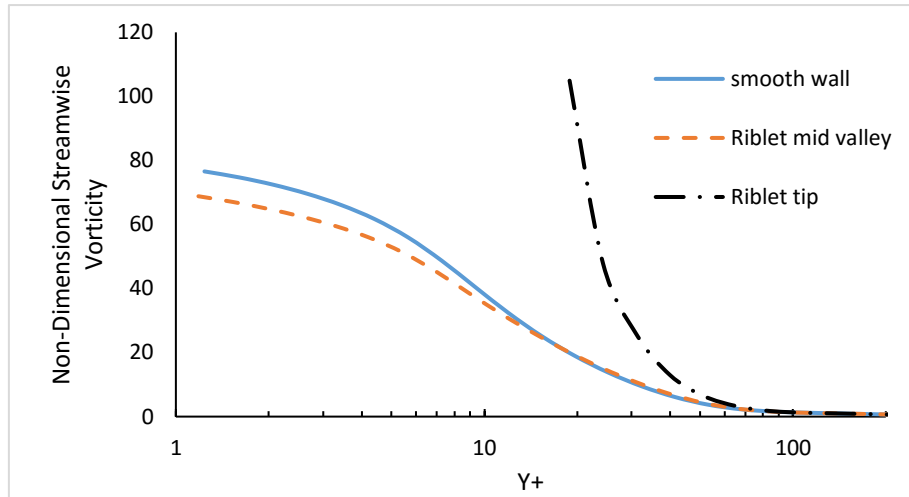
Figure (13): mass averaged streamwise vorticity at 40% stream-wise location

To evaluate the effect of increasing the vorticity at riblets tips on skin friction, the wall shear was calculated along the hub surface at the 40% plane. Figure 14 reveals that increasing the vorticity at riblets tips increases the wall shear at small areas around the tips, while the wall shear inside the riblets valley is reduced keeping the average shear below that for the smooth surface.
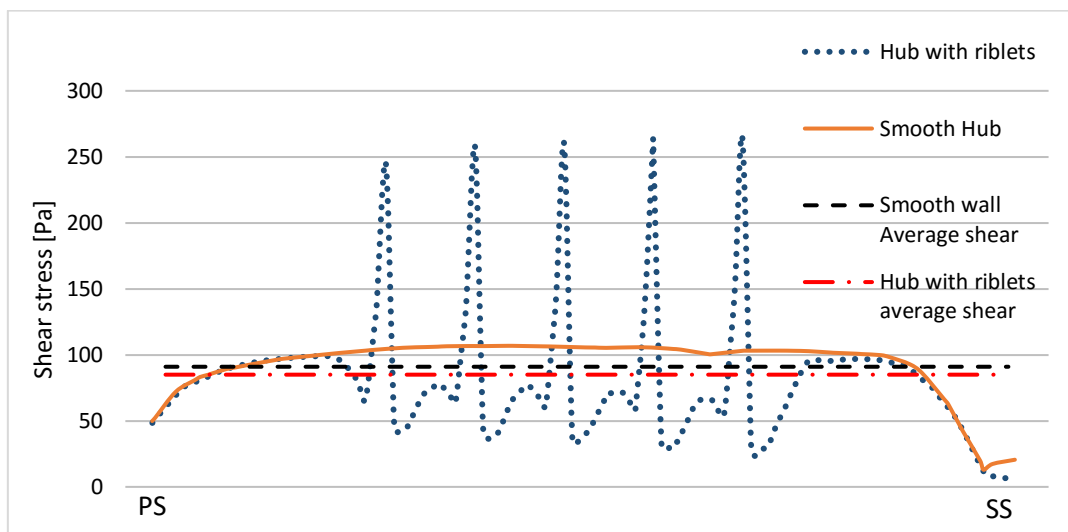

Figure (14): wall shear at the hub surface calculated at 40% stream-wise location

The turbulent kinetic energy profiles over smooth hub, riblets valley and riblet tip are plotted in figure 15. It is obvious that introducing the riblets to the hub surface damps the velocity components fluctuations leading to reduction in turbulent kinetic energy. Chun et al. [4], Lee et al. [18] and Duan [19] have spotted similar drop in turbulent kinetic energy when riblets were introduced to flat plate surfaces.
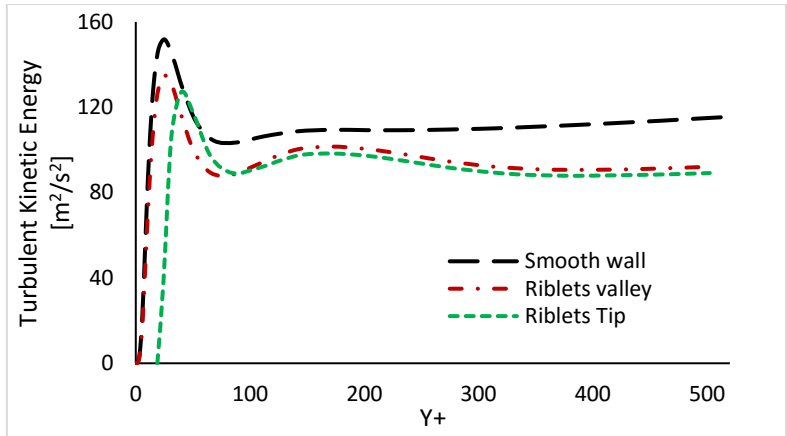
Figure (15): comparison of turbulent kinetic energy for both smooth rotor and rotor with riblets

1.3.3 Riblets Geometry Effect

In this section the effect of different riblets geometries (refer to table 2) on drag reduction is examined and compared with the smooth wall results. Figure 16 compares the area averaged shear at the hub surface for the riblets with different height and spacing. The results reveal that the spacing between riblets has a minor effect on the wall shear stress reduction and the key parameter that affects the riblets performance is their height. The highest drag reduction was achieved using riblet with relative height 2.5%, whilst increasing riblet height to 5% has a negative impact, where drag increases at the hub surface.
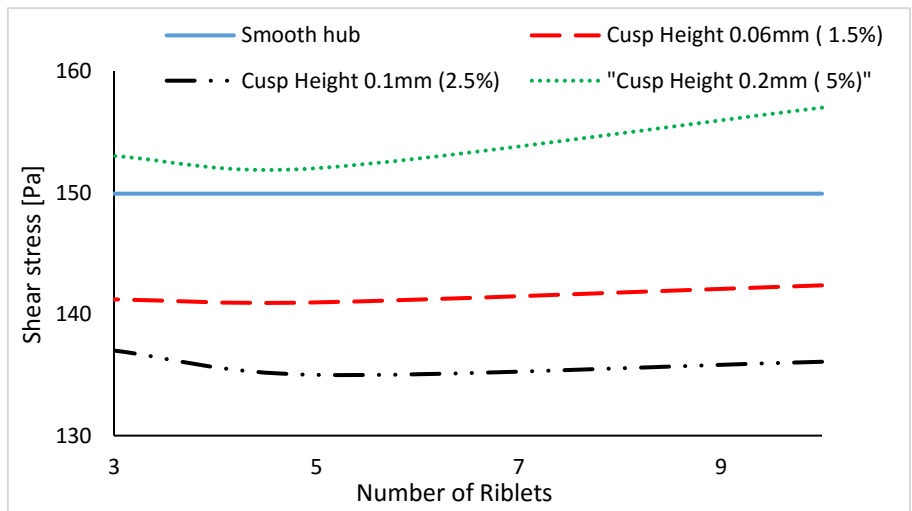

Figure (16): Wall shear stress comparison between different riblets geometries

Most of the research studies performed on the riblets set geometrical conditions on riblets performance. According to those studies; riblets reduces drag for normalised spacing $s^+ < 30$ and normalised height $h^+ < 25$ wall units. Figure 17 presents the change in drag ($\Delta \tau$ defined in eq. 2) for riblets with different spacing s^+ and constant height ($h_{rel} = 2.5$, $h^+ = 19.3$).

$$\Delta\tau = (\tau_r - \tau_s)/\tau_s \hspace{3cm} (2)$$

Where, τ_s and τ_r are the wall shear stresses at the smooth and ribbed hub surfaces respectively. The graph shows that the spacing s+ has a negligible effect on riblets performance, it shows also that riblets can reduce drag for high values up to 300 wall units. This conflicts with the values in literature and the value presented here is mainly due to the type of the flow. Most of the available experimental data that limits riblet spacing to 30 wall unit are done for external flows. This is directly related to the streamwise vorticity at body surface, where size of the streamwise vortices for external flows is about 30 wall units in diameter. Therefore, increasing the space between riblets to more than that will provide the freedom for the streamwise vortex to move freely in the area between them. This will cause increment in area exposed to high speed cross flow which in turn increases skin friction [18]. On the other hand, the streamwise vortex at the turbine hub occupies almost the whole passage width, therefore increasing the spacing s^+ didn't change the performance of the riblets (see figure 13).
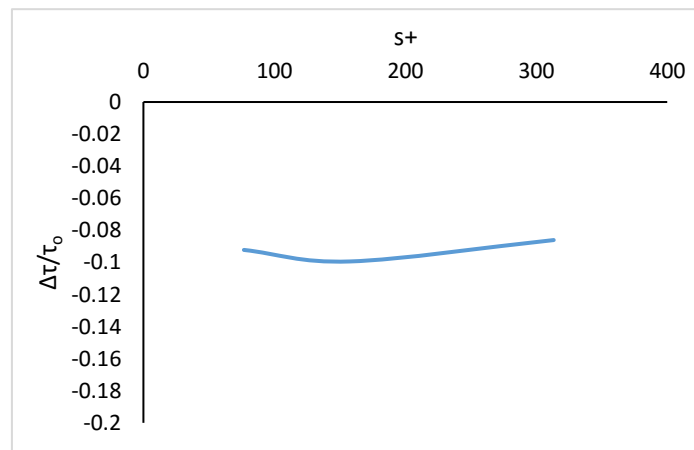

Figure (17): drag reduction for different riblets spacing

Figure 18 presents the change in drag for different riblets height h^+ at constant rib spacing (s = 0.039r_{hub}, s^+ =158). Wall shear using riblets is reduced until reaching the rib height (h^+ = 19.3) where the wall shear is minimum, while increasing riblets height further leads to increase the wall shear. A similar trend for riblets performance within internal flows was spotted by Lei et al. [1], where the drag reduction was found to be related to riblet height. Increasing riblets height increases the generation of secondary vortices which increases the down washing motion of the high-speed fluids around riblet tip causing more drag.
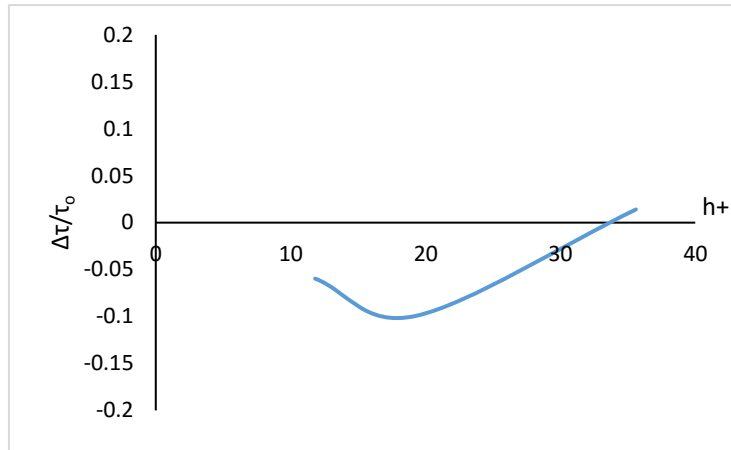
Figure (18): drag reduction for different riblets spacing

Figure 19 shows the mass averaged streamwise vorticity along the turbine passage. The graph shows that increasing the height of the riblets increases the streamwise vorticity along the passage. This explains the performance results in figure 20 where the turbine with riblets of height h_{rel} =1.5% has a higher efficiency than h_{rel} = 2.5% even the latest shows better performance in reducing drag.
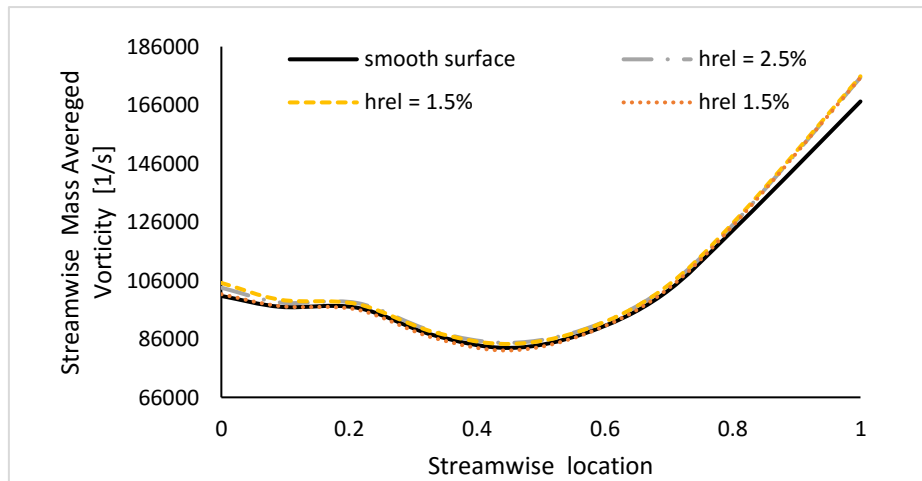

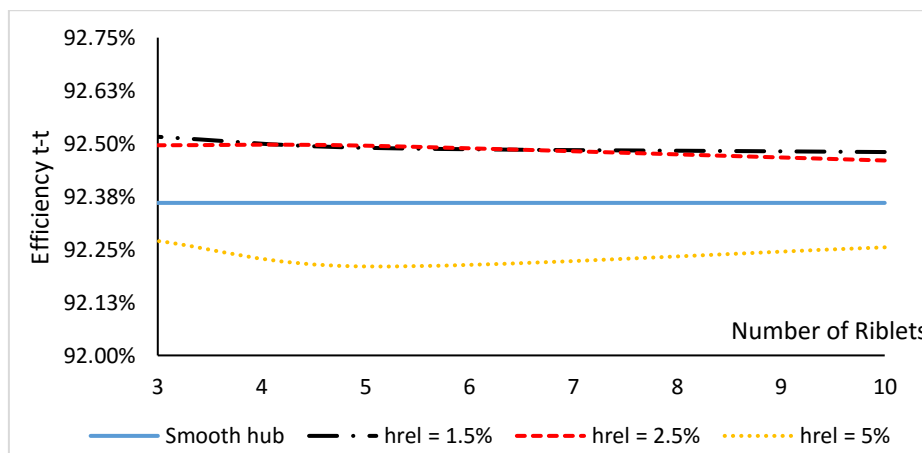Figure (19): Mass averaged streamwise vorticity along rotor passage

Figure (20): Turbine performance for different riblets geometry

Conclusion

In this work the effects of residual riblets on radial turbine performance were analysed numerically. It was found that residual riblets reduce the cross-stream motion of the low momentum fluids leading it to move from pressure to suction side of the rotor passage and separate the streamwise vortex from interaction with hub surface. This entrains low speed fluid in the riblets valley which in turn reduces the momentum transfer in the boundary layer causing reduction in wall shear stress.

The spacing between riblets was found to be of secondary effect on their performance in drag reduction as the streamwise vortex occupies most of the passage length. Riblets height was found to be the main parameter affecting drag reduction, where the maximum drag reduction found to occur with riblets with $h_{rel} = 2.5\%$. Introducing riblets to hub surface is beneficial for drag reduction while it increases the streamwise vorticity in the rotor passage and the maximum performance was achieved for the turbine with the shortest riblets ($hrel = 1.5\%$). Future work will focus on studying the effect of riblets on the turbine performance at off-design conditions.

Nomenclature

Y+	Non-dimensional wall distance: $Y^+ = \frac{Y u_\tau \rho}{\mu}$
s+	Non-dimensional spacing between riblets: $s^+ = \frac{s u_\tau \rho}{\mu}$
h+	Non-dimensional riblets height: $h^+ = \frac{h u_\tau \rho}{\mu}$
u_τ	Friction velocity: $\sqrt{\tau_o / \rho}$
τ_o	Wall Shear
ρ	Density
ω	Rotational speed
r	radius
P_s	static pressure
P_r	reduced static pressure

References

[1] D. Lei and L. Cao, "Effects of Residual Ribles of Impeller's Hub Surface on Aerodynamic Performance of Centrifugal Compressors," *Engineering Applications of Computational Fluid Mechanics,* vol. 9, pp. 99-113, 2005.

[2] M. Walsh, "Turbulent Boundary Layer Drag Reduction Using Riblets," in *20th Aerospace Sciences Meeting*, Orlando, 1980.

[3] M. Walsh, "Riblets as a Viscous Drag Reduction Technique," *AAIA Journal,* vol. 21, pp. 485-486, 1983.

[4] H. Chun, O. El-Samni and H. Yoon, "Drag Reduction of Turbulent Flow over Thin Rectangular Riblets," *International Journal of Engineering Science,* vol. 45, pp. 436-454, 2007.

[5] K. Oehlert and J. Seume, "Exploratory Experiments on Machined Riblets on Compressor Blades," in *ASME Fluids Engineering Division*, Miami, 2006.

[6] C. Fang , C. Zhang and T. Ping, "An Experimental Investigation of Loss Reduction with Riblets on Cascade Blade Surface and Isolated Airfoils," in *ASME Gas Turbine Division*, New York, 1990.

[7] B. Bhushan and B. Dean, "The Effect of Riblets in Rectangular Duct Flow," *Applied Surface Science,* vol. 258, no. 8, pp. 3936-3947, 2012.

[8] Z. Q, X. Miao, L. Wang, J. H and H. Qi, "Application of Riblets on Turbine Blade End-wall Secondary Flow Control," *Journal of Propulsion and Power,* vol. 31, pp. 1578-1585, 2015.

[9] K. Kim, J. Cho, J. Kim and E. Jeong, "Controlling the Secondary Flows Near Endwall Boundary Layer Fences in a 90° Turning Duct Using Approximate Optimization Method," *Journal of Mechanical Science and Technology,* vol. 25, pp. 2025-2034, 2011.

[10] X. Miao, Z. Sun, Q. Zhang and C. Atkins, "End-wall Seconary Flow Control Using Engineering Residual Surface Structure," in *ASME Turbo Expo*, Seoul, 2016.

[11] J. Dai, N. Ijichi, H. Tange, H. Shibata, H. Tamaki and S. Yamaguchi, "Comparison of internal flow field between experiment and computation in a radial turbine impeller," *JSME international Journal,* vol. 47, pp. 48-56, 2004.

[12] J. E. Bardina, P. G. Huang and T. J. Coakley, "Turbulence Modeling Validation, Testing, and Development," Ames Research Center, Moffett Field, California, 1997.

[13] Q. Deng, J. Niu and Z. Feng, "Study on the leakage flow characteristics of radial inflow turbines at rotor tip clearance," *Science in China Series E: Technological Sciences,* vol. 51, 2008.

[14] A. Jones, "Design and Test of a Small, High Pressure Ratio Radial Turbine," in *ASME int. gas turbine congress*, Netherlands, 1994.

[15] Z. Sun, C. Guo, H. Chen and C. Tan, "Aerothermal Investigation of Backface Clearance Flow in Deeply Scalloped Radial Turbines," *Journal of Turbomachinery,* vol. 135, 2013.

[16] E. M. Greitzer, C. Tan and M. B. Graf, Inetrnal Flow: Concepts and Applications, Cambrige University Press, 2007.

[17] M. Zangeneh-Kazemi, W. Dawes and W. R. Hawthorne, "Three Dimensional Flow in Radial-Inflow Turbines," in *Gas Turbine and Aeroengines Congress*, Amsterdam, 1988.

[18] S. J. Lee and S. H. Lee, "Flow Field Analysis of Turbulent Boundary Layer Over A Riblet Surface," *Experiments in Fluids Springer,* vol. 30, pp. 153-166, 2001.

[19] L. Duan, "Effects of Ribelts on Skin Friction in High-Speed Turbulent Boundary Layers," in *AIAA 50th* , Nashville, 2012.